

# Discovery of Quasi-Integrable Equations from traveling-wave data using the Physics-Informed Neural Networks

A. Nakamura,<sup>1,\*</sup> N. Sawado,<sup>2,†</sup> K. Shimasaki,<sup>2,‡</sup> Y. Shimazaki,<sup>2,§</sup> Y. Suzuki,<sup>2,¶</sup> and K. Toda<sup>3,4,\*\*</sup>

<sup>1</sup>*Department of Physics, School of Science,*

*Kitasato University, Sagamihara, Kanagawa 252-0373, Japan*

<sup>2</sup>*Department of Physics and Astronomy, Tokyo University of Science, Noda, Chiba 278-8510, Japan*

<sup>3</sup>*Department of Mathematical Physics, Toyama Prefectural University, Imizu, Toyama 939-0398, Japan*

<sup>4</sup>*Research and Education Center for Natural Sciences, Keio University,*

*Hiyoshi 4-1-1, Yokohama, Kanagawa 223-8521, Japan*

Physics-Informed Neural Networks (PINNs) are used to study vortex solutions in the 2+1 dimensional nonlinear partial differential equations. These solutions include the regularized long-wave (RLW) equation and the Zakharov-Kuznetsov (ZK) equation, which are toy models of the geostrophic shallow water model in the planetary atmosphere. PINNs successfully solve these equations in the forward process and the solutions are obtained using the mesh-free approach and automatic differentiation while accounting for conservation laws. In the inverse process, the proper equations can be successfully derived from a given training data. Since these equations have a lot in common, there are situations when substantial misidentification arises during the inverse analysis. We consider PINNs with conservation laws (referred to as cPINNs), deformations of the initial profiles, and a friction approach that provides excellent discrimination of the equations to improve the identification's resolution.

## I. INTRODUCTION

Application of deep learning techniques in the form of deep neural networks to the nonlinear partial differential equations (PDEs) have gained much attention in recent years. The Physics-Informed Neural Networks (PINNs) [1–3] have the ability to solve many complicated scientific problems such as fluid and solid mechanics [4–9], cyber-physical systems [10], biological systems [11–14], and many others. One unique, noteworthy aspect of the PINNs is not only their ability to efficiently solve PDEs (the forward analysis) but also to provide us with an accurate estimate of the equation based on the governing data of the physical problems of our concern (the inverse analysis).

\* nakamura@sci.kitasato-u.ac.jp

† sawadoph@rs.tus.ac.jp

‡ shimasakitus@gmail.com

§ shimazakitus@gmail.com

¶ ytszkyuta@gmail.com

\*\* kouichi@yukawa.kyoto-u.ac.jp

In general, PINNs have significantly higher extrapolation power compared to other conventional deep-learning techniques, making them appropriate for analyses involving limited learning data. Recently, there have been some attempts to apply the methods into more complex geometry of data [15, 16].

It should be noted that PINNs is distinct from the conventional, standard numerical algorithm [17–21] that uses the finite difference method and finite element method, where the governing PDEs are eventually discretized over the computational domain. Providing a mesh-free approach is one of the main benefits of PINNs, since automatic differentiation approximates the differential operators in the governing PDEs. Traditional numerical approaches strongly depend on a number of grids, which may cause a curse of dimensionality. On the other hand, PINNs’ grid independence is undoubtedly efficient particularly for solving high-dimensional problems and inverse analysis. An additional benefit of utilizing PINNs is their ability to integrate conservation laws of a system into analysis by incorporating the condition into the loss function. The method called cPINNs gains the accuracy of the analysis [17, 22, 23].

Since the methods’ original premise involved application to fluid mechanics with PDEs [4, 5] and a weather/climate modelling [8], it is natural to extend the analysis into the large dynamics of planetary atmospheres, such as Jupiter’s or other planets, hopefully, described by some nonlinear PDEs. In this context, the Great Red Spot (GRS) of Jupiter is an illustration of a unique, extraordinary object because of its amazing longevity. Its stable nature strongly suggests that there are unknown mechanisms that emerged from the highly non-linear character of dynamics. Many observations indicate the phenomenon is certainly shallow in its depth of the atmosphere [24]. Models of shallow water equation and (or) its induced effective equations in several geostrophic regimes may possibly describe for physics of the GRS. Charney-Hasegawa-Mima (CHM) equation [25] in quasi-geostrophic regime and Williams-Yamagata-Flierl (WYF) equation [26–28] in intermediate geostrophic regime look promising candidates. The crucial step in solving various physical problems is to choose the appropriate governing equation. There are numerous potential possibilities for the GRS, but as far as we are aware, there is still no ideal equation.

In the present paper, we solve quasi-integrable equations via PINNs as reduced, toy models, instead of directly solving the geostrophic equations mentioned above. Recently, a dramatic increase in computing power has become effective to bear on these problems directly in simulation technology. A drawback of this approach is the lack of a simple analytical framework that can help in the interpretation of numerical results. The above geostrophic equations give us many insights into the phenomena and the traditional approaches can of course work for the analysis of

these equations. One advantage of solving the integrable, or the quasi-integrable counterparts is to expose the primary character of the phenomena which is usually described by some mathematical language such as the existence of (infinite number of) conservation quantities. There are numerous studies of PINNs for the integrable equations, such as the Bergurs eq. [1–3, 17, 22], the KdV eq. and the modified KdV eq. [17, 29–33], the nonlinear Schrödinger eq. [34, 35], and many other variations. In 2+1 dimensions, the KP eq. and the spin-nonlinear Schrödinger eq. were studied via PINNs [36–38], respectively. There are several studies for quasi-integrable deformation of the KdV eq. [39, 40], rogue-waves in the nonlinear Schrödinger eq. [41–44] and some field theoretical models such as the massive Thirring model [45].

The objective of the present paper is to apply PINNs to two quasi-integrable equations, Zakharov-Kuznetsov (ZK) equation and the regularized long-wave (RLW) equation, which are reduced model of the above fluid mechanical equations. The ZK eq. [46, 47] is a direct extension of the KdV equation into higher dimensions. At the moment the researches [47–49] have focused on the two-dimensional version of the model. The equation possesses stable isolated vortex-type solutions which enjoy solitonic properties. It is well known that some inelastic properties emerge when the heights of vortices are significantly different, in a collision process the taller soliton gains more height while the shorter one tends to wane with the radiation [47]. The RLW eq. [50, 51] is a shallow-water fluid model to simulate the development of an undular bore. The RLW equation in two dimensions possesses a stable isolated vortex solution [52]. The peculiar inelastic properties of the solitons have been extensively studied in the literatures [53–55] in 1+1 dims. and also [52] in 2+1 dims. of the equations. In PINNs' inverse analysis, there are situations when substantial misidentification between the vortex solutions of the ZK and the RLW equations arises. That is, when the candidate equation has terms from both the ZK and the RLW, we are unable to determine the governing equation in the inverse PINNs. These equations have a lot in common, for example, they have the same number of conserved quantities and possess the same form of traveling wave solution. It appears to be the origin of the substantial misidentification that could happen in PINN inverse analysis. In the present paper, we will provide several resolutions for avoiding the problem.

The present paper is based on the proceeding paper of *the XII. International Symposium on Quantum Theory and Symmetries (QTS12)* [56]. In the proceeding, we presented a few potential solutions to the problem, including variations of the initial conditions and a friction method in terms of the  $y$ -dependent sheared current, which will be thoroughly covered in the present paper. The approach is undoubtedly improved in this paper, and we obtain excellent convergent properties

of the mean squared error, which was not looked at in the previous study. In this paper, we will introduce a new friction that certainly improves the identification ability than that of the term considered in the proceeding. We also focus on the cPINNs analysis and the use of the two-soliton solutions for the inverse analysis, which are the inventive contents in the present paper.

The paper is organized as follows. In Section II, we give a brief introduction of the Zakharov-Kuznetsov equation and the regularized long-wave equation. The derivation of the conservation quantities in these equations are done in this section. We present an overview of Physics Informed Neural Networks in Section III. We demonstrate the misidentification of the solutions as well as the good performance of PINNs for the quasi-integrable equations. We provide several (less-effective) prescriptions to avoid the problem. In Section IV, we give successful solutions, in which we introduce variations of the initial conditions and also a small perturbation for the equations and show how they work well. The conclusions and remarks are presented in the last section.

## II. (2 + 1) QUASI-INTEGRABLE SYSTEM AND THE STABLE VORTICES

Though the term “quasi-integrability” is frequently employed in literature, mathematically it is still a bit obscure. One nice straightforward definition of a quasi-integrable system is a PDE that has only a finite number of exact conservation quantities. We will investigate the quasi-integrable systems from this simple perspective, whose solutions resemble solitons in the integrable system, and have just four conservation quantities. This paper investigates a well-known quasi-integrable system in two space dimensions that embody the underlying KdV dynamics for the stability of their vortex solutions. The PINNs analysis detects a signal resulting from partial conservation of the quantities, which will be seen in the next section. In [55, 57], the authors give more thorough discussions about concept of the quasi-integrability.

### A. Zakharov-Kuznetsov equation

The Zakharov-Kuznetsov (ZK) equation

$$\frac{\partial u}{\partial t} + 2u \frac{\partial u}{\partial x} + \frac{\partial}{\partial x} (\nabla^2 u) = 0 \quad (1)$$

originally was the model in three dimensions of plasma with a uniform magnetic field [46]. Since most of the later researches [47–49] have focused on the two-dimensional version of the model, the Laplacian specifies  $\nabla^2 = \partial_x^2 + \partial_y^2$ . Eq.(1) possesses meta-stable isolated vortex-type solutions which enjoy the solitonic properties. The single soliton is dynamically stable, and the two solitons of equal

height appear to collide without merging or dissipating, similar to the ones in the well-known KdV solitons. This does not apply to the two solitons, whose heights are significantly different. The taller soliton is increased while the shorter one tends to wane with the radiation [47].

The equation possesses the solutions propagating in a specific direction with uniform speeds. Here we set the direction in the positive  $x$  orientation with velocity  $c$ , namely assuming  $u = U(\tilde{x} := x - ct, y)$ . Plugging it into (1), we obtain

$$\nabla^2 U = cU - U^2, \quad (2)$$

where  $\nabla^2 = \partial_{\tilde{x}}^2 + \partial_y^2$ . A steady progressive exact wave solution is of the form

$$U_{1d} = \frac{3c}{2} \operatorname{sech}^2 \left[ \frac{\sqrt{c}}{2} (\tilde{x} \cos \theta + y \sin \theta) \right], \quad (3)$$

where the  $\theta$  is a given inclined angle of the solution. It indicates that this solution is just a trivial embedding of the KdV soliton into two spatial dimensions. Eq.(2) possesses another solution keeping circular symmetry other than (3). To find it, we introduce cylindrical coordinates and rewrite the equation as

$$\frac{1}{r} \frac{d}{dr} \left( r \frac{dU(r)}{dr} \right) = cU(r) - U(r)^2, \quad (4)$$

where  $r := \sqrt{\tilde{x}^2 + y^2}$ . We can find the solutions with the boundary condition  $U \rightarrow 0$  as  $r \rightarrow \infty$  numerically and the solutions form one parameter family of  $c$  such as  $U(r) := cF(\sqrt{c}r)$ .

The solutions of (1) exhibit soliton-like; however, they are not similar to the solitons in integrable systems as those of the KdV equation, in that the stability of the solutions may be supported by the infinite number of conserved quantities in the equation. Eq.(1) admits only the four integrals of motion [58], which are

$$I_1 := \int i_1(y) dy = \int u dx dy, \quad i_1(y) := \int u dx, \quad (5)$$

$$I_2 := \int \frac{1}{2} u^2 dx dy, \quad (6)$$

$$I_3 := \int \left[ \frac{1}{2} (\nabla u)^2 - \frac{1}{3} u^3 \right] dx dy, \quad (7)$$

$$I_4 := \int \mathbf{r} u dx dy - t \mathbf{e}_x \int u^2 dx dy, \quad (8)$$

where  $\mathbf{r}$  and  $\mathbf{e}_x$  is the two-dimensional position vector and the unit vector in the  $x$ -direction. Here  $I_1$  is interpreted as the ‘‘mass’’ of the solution, and  $I_1(y)$  itself is conserved similarly to the KdV equation, respectively. Also,  $I_2, I_3, I_4$  means the momentum, the energy, and the laws for the center of mass, respectively. We, therefore, conclude that the ZK equation is not an integrable system in the manner of ordinary soliton equations.

### B. The regularized long-wave equation

The regularized long wave (RLW) equation was introduced by Peregrine [50] to simulate the development of the undular bore in the shallow water system and many analytical and numerical studies have followed such as [51, 52, 59–63]. The two-dimensional version of the RLW equation

$$\frac{\partial u}{\partial t} + \frac{\partial u}{\partial x} + u \frac{\partial u}{\partial x} - \frac{\partial}{\partial t} (\nabla^2 u) = 0 \quad (9)$$

concerns the drift waves in magnetized plasma or the Rossby waves in rotating fluids, where the field  $u$  describes the mean horizontal velocity of the water.

It is noteworthy that, for the steady traveling solutions, the RLW equation and the ZK equation have similar fundamental properties in that, when we plug  $u = U(\tilde{x}, y)$  into (9), we promptly get

$$c\nabla^2 U = (c-1)U - \frac{1}{2}U^2. \quad (10)$$

In fact, by the transformations

$$\text{for ZK eq.: } U = cF(X, Y), \quad X := \sqrt{c}\tilde{x}, \quad Y := \sqrt{c}y, \quad (11)$$

$$\text{for RLW eq.: } U = 2(c-1)F(X, Y), \quad X := \sqrt{1 - \frac{1}{c}}\tilde{x}, \quad Y := \sqrt{1 - \frac{1}{c}}y \quad (12)$$

respectively, eqs.(2) and (10) reduce to a normalized identical equation

$$\nabla^2 F - F + F^2 = 0, \quad \nabla^2 := \partial_X^2 + \partial_Y^2. \quad (13)$$

Our central concern in the paper is that coincidence often brings misidentification into the PINNs analysis. Another similarity between the two equations is that the RLW equation also has the four conserved quantities, albeit with somewhat different forms

$$\bar{I}_1 := \int \bar{i}_1(y) dy = \int u dx dy, \quad \bar{i}_1(y) := \int u dx, \quad (14)$$

$$\bar{I}_2 := \int [(\nabla u)^2 + u^2] dx dy, \quad (15)$$

$$\bar{I}_3 := \int \left( \frac{1}{2}u^2 + \frac{1}{6}u^3 \right) dx dy, \quad (16)$$

$$\bar{I}_4 := \left[ \mathbf{r}u + \mathbf{e}_x \frac{1}{2} \int_{t_0}^t (\nabla u)^2 dt' \right] dx dy - t \mathbf{e}_x \int \left\{ u + \frac{1}{2} [u^2 + (\nabla u)^2] \right\} dx dy, \quad (17)$$

The  $\bar{I}_2$  is now the result of energy conservation, not the third quantity  $I_3$  of the ZK equation.

### III. PRELIMINARY ANALYSIS

The PINNs deep learning method is the most effective at solving initial-boundary problems (forward problems) and reconstructing equations (inverse problems), as it can find the governing equation from given data. In the following, we introduce the PINNs method solving data-driven vortex (2+1) solutions of the non-linear quasi-integrable differential equations.

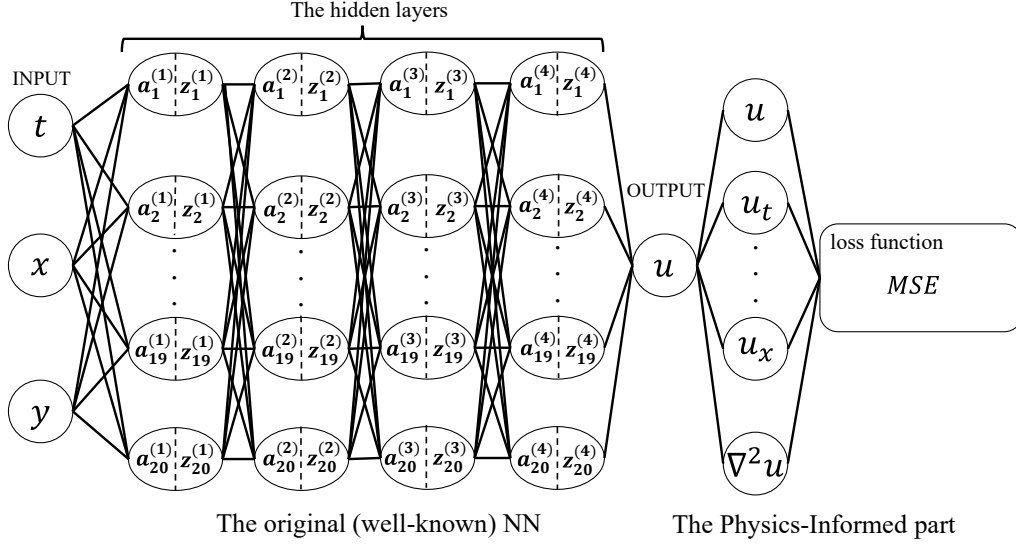


FIG. 1. The PINNs: In the first part, we first calculate the weight sum,  $a_m^{(n)} = \sum_{i=1}^{20} \{w_{im}^{(n)} z_i^{(n-1)} + b_m^{(n)}\}$  where  $(w_{lk}^{(j)}, b_k^{(j)})$  are the weight parameters. Second, we use  $\tanh x$  as the activation function. Finally, the output is obtained through the hidden layers. After that, in the second part, we calculate the derivatives and construct a loss function.

#### A. The PINNs for the (2+1)-dimensional quasi-integrable systems

The method consists of two parts of the networks. The first segment is the well-known neural networks part, which is constructed with 4 hidden layers and 20 nodes for which each layer to get the output  $u$  from the inputs, time-spatial coordinates  $(t, x, y)$ . However, the output of this network has no physical meaning. In the second segment, the output derivatives and a loss function for network optimization are estimated (see sections 3.2 and 3.3 in detail).

The PINNs can be applied to both forward and inverse problems. The forward analysis is that

one can solve a governing equation and find the solutions without large computational resources or sophisticated numerical algorithms. Let us consider the PDEs

$$\text{ZK eq: } \mathcal{F}_{\text{ZK}} := u_t + \mathcal{N}_{\text{ZK}}(u, u_x, u_{xxx}, u_{xyy}) = 0, \quad (18)$$

$$\text{RLW eq: } \mathcal{F}_{\text{RLW}} := u_t + \mathcal{N}_{\text{RLW}}(u, u_x, u_{txx}, u_{tyy}) = 0, \quad (19)$$

where  $\mathcal{N}_{\text{ZK}}$ ,  $\mathcal{N}_{\text{RLW}}$  are non-linear functions which are defined by

$$\mathcal{N}_{\text{ZK}}(u, u_x, u_{xxx}, u_{xyy}) := 2uu_x + (\nabla^2 u)_x, \quad (20)$$

$$\mathcal{N}_{\text{RLW}}(u, u_x, u_{txx}, u_{tyy}) := 2uu_x + (\nabla^2 u)_t, \quad (21)$$

respectively. For simplicity, we have removed the term  $u_x$  from the RLW equation. It is not equivalent to the RLW equation in a strict sense. As the equation without the term reduces to the same normalized equation (13), a numerical traveling-wave solution still exists. We focus on the vortex solutions moving to the positive  $x$  direction in these equations. We define the rectangular mesh space

$$\begin{aligned} x &\in [-L_x, L_x], N_x \text{th grid points; } & y &\in [-L_y, L_y], N_y \text{th grid points,} \\ t &\in [T_0, T_1] \end{aligned} \quad (22)$$

For optimization of the networks, the mean-squared error function:  $MSE$  is implemented as the loss function to measure the discrepancy between the predicted values and the correct ones, which can be chosen such that

$$MSE = \frac{1}{N_u} \sum_{i=1}^{N_u} |u_{\text{pred}}^0(x^i, y^i, 0) - u_{\text{correct}}^0(x^i, y^i, 0)|^2 + \frac{1}{N_F} \sum_{i=1}^{N_F} |\mathcal{F}(x^i, y^i, t^i)|^2 + \frac{1}{N_b} \sum_{N_b} |BC|^2, \quad (23)$$

where  $u_{\text{pred}}^0$  is the predicted initial profile,  $u_{\text{correct}}^0$  is the correct initial profile,  $\{x^i, y^i, 0\}_{i=1}^{N_u}$  is the set of  $N_u$ th random residual points, and  $\{x^i, y^i, t^i\}_{i=1}^{N_F}$  is the  $N_F$ th random points for the PINNs  $\mathcal{F}(x, y, t)_{\text{ZK}}$  or  $\mathcal{F}(x, y, t)_{\text{RLW}}$ . Finally,  $BC$  represents mean squared error caused by the boundary conditions with the random  $N_b$ th points. Here, the doubly periodic boundary conditions are employed as

$$\begin{aligned} \sum_{N_b} |BC|^2 &= \sum_{i=1}^{N_{b,x}} |u_{\text{pred}}(x^i, L_y, t^i) - u_{\text{pred}}(x^i, -L_y, t^i)|^2 \\ &+ \sum_{j=1}^{N_{b,y}} |u_{\text{pred}}(L_x, y^j, t^j) - u_{\text{pred}}(-L_x, y^j, t^j)|^2. \end{aligned} \quad (24)$$

where  $N_b \equiv N_{b,x} + N_{b,y}$ . When the MSE goes to 0, the output  $u$  reaches the exact solution of the PDE. In Fig.2, we present the typical solution of the ZK equation in terms of the forward analysis.

Another prominent application of PINNs is the creation of the PDE from provided data. Now, we introduce a slightly modified PINNs

$$\text{ZK eq: } \tilde{\mathcal{F}}_{\text{ZK}} := u_t + \tilde{\mathcal{N}}_{\text{ZK}}(u, u_x, u_{xxx}, u_{xyy}, \boldsymbol{\lambda}) = 0, \quad (25)$$

$$\text{RLW eq: } \tilde{\mathcal{F}}_{\text{RLW}} := u_t + \tilde{\mathcal{N}}_{\text{RLW}}(u, u_x, u_{txx}, u_{tyy}, \boldsymbol{\lambda}) = 0, \quad (26)$$

where the unknown parameters  $\boldsymbol{\lambda}$  is implemented in the equations. For the inverse analysis, we employ the other MSE as

$$\text{MSE} = \frac{1}{N_u} \sum_{i=1}^{N_u} |u_{\text{pred}}(x^i, y^i, t^i) - u_{\text{correct}}(x^i, y^i, 0)|^2 + \frac{1}{N_F} \sum_{i=1}^{N_F} |\tilde{\mathcal{F}}(x^i, y^i, t^i)|^2, \quad (27)$$

where  $u_{\text{pred}}$  is the predicted profile and  $u_{\text{correct}}$  is the correct profile including the boundary data. Varying the parameters of the Neural Networks  $(w_{lk}^{(j)}, b_k^{(j)})$  and also the parameters  $\boldsymbol{\lambda}$ , the networks are properly optimized. As a result, we obtain the proper  $\boldsymbol{\lambda}$  and then the idealized equations for corresponding training data.

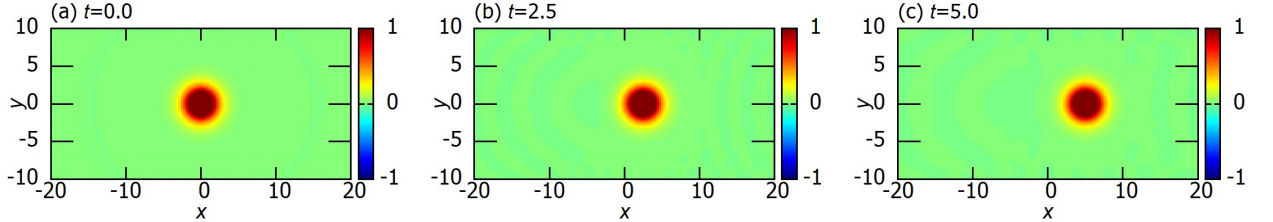


FIG. 2. The solution of the ZK equation in the forward PINNs analysis.

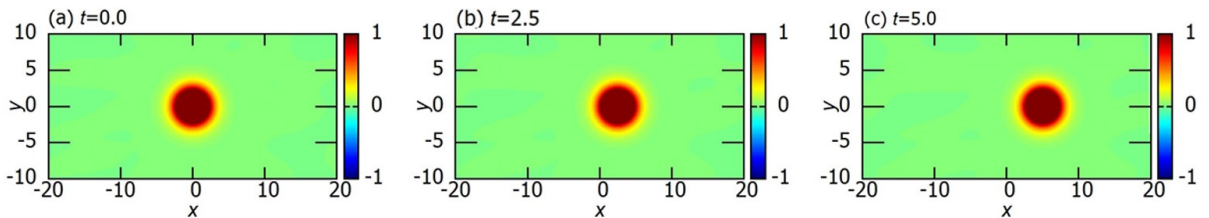


FIG. 3. The solution of the RLW equation in the forward PINNs analysis.

TABLE I. *The successful* parameterization for the ZK equation.

	<i>PDE</i>	<i>MSE</i> ( $\times 10^{-6}$ )
Correct equation	$u_t + 2uu_x + (\nabla^2 u)_x = 0$	–
Identified (1)	$u_t + 2.046uu_x + 1.0048 (\nabla^2 u)_x = 0$	4.4
Identified (2)	$u_t + 2.011uu_x + 1.0033 (\nabla^2 u)_x = 0$	4.6

TABLE II. *The successful* parameterization for the RLW equation.

	<i>PDE</i>	<i>MSE</i> ( $\times 10^{-6}$ )
Correct equation	$u_t + uu_x - (\nabla^2 u)_t = 0$	–
Identified (1)	$u_t + 0.9999uu_x - 0.9996 (\nabla^2 u)_t = 0$	1.3
Identified (2)	$u_t + 0.9989uu_x - 0.9981 (\nabla^2 u)_t = 0$	1.4

### B. Successful analyses for the ZK equation and the RLW equation

As a demonstration, we employ the PINNs for solving evolution equations and the solutions that are found in the profile  $u$ 's training data. We define  $\tilde{\mathcal{N}}$  for the inverse analysis for the ZK equation, using two unknown constants  $\lambda_0, \lambda_1$

$$\tilde{\mathcal{N}}_{\text{ZK}}(u, u_x, u_{xxx}, u_{xyy}; \lambda_0, \lambda_1) := \lambda_0 uu_x + \lambda_1 (\nabla^2 u)_x. \quad (28)$$

We investigate the inverse analysis of the PINNs for finding the parameter values  $(\lambda_0, \lambda_1)$  in terms of the training data derived from the forward analysis. In the PINNs analysis, the numerical uncertainty is an inevitable consequence of training data sampling. We establish the correctness of our research in this paper by using the prescription of doing double identification for the same training data. In Table I, we present the result of the inverse analysis for the Zakharov-Kuznetsov equation. One can see that the PINNs method reproduces the governing equation from the training data. For the RLW equation, the PINN  $\tilde{\mathcal{N}}$  is defined as

$$\tilde{\mathcal{N}}_{\text{RLW}}(u, u_x, u_{txx}, u_{tyy}, \lambda_0, \lambda_1) := 2\lambda_0 uu_x + \lambda_1 (\nabla^2 u)_t \quad (29)$$

In the following, we shall omit the term  $u_x$  in the equation for the simplicity. The result of the PINNs inverse analysis is presented in Table II.

The PINN functions  $\tilde{\mathcal{N}}_{\text{ZK}}$  (28),  $\tilde{\mathcal{N}}_{\text{RLW}}$  (29) are taken into account just the same contents as the function of the forward analysis  $\mathcal{N}_{\text{ZK}}$  (20),  $\mathcal{N}_{\text{RLW}}$  (21), which is what makes the PINNs analysis successful as shown here. Such an excellent predictive power is often lost when we try to introduce a

TABLE III. The *misidentification* for the ZK equation.

	PDE	MSE ( $\times 10^{-6}$ )
Correct equation	$u_t + 2uu_x + 0.0 (\nabla^2 u)_t + (\nabla^2 u)_x = 0$	—
Identified $c = 2(1)$	$u_t + 2.0011uu_x - 0.4017 (\nabla^2 u)_t + 0.2019 (\nabla^2 u)_x = 0$	3.8
Identified $c = 2(2)$	$u_t + 2.0015uu_x - 0.4796 (\nabla^2 u)_t + 0.0116 (\nabla^2 u)_x = 0$	4.0
Identified $c = 1(3)$	$u_t + 2.0048uu_x - 0.5190 (\nabla^2 u)_t + 0.5311 (\nabla^2 u)_x = 0$	4.1
Identified $c = 1(4)$	$u_t + 2.0452uu_x - 0.61035 (\nabla^2 u)_t + 0.4358 (\nabla^2 u)_x = 0$	5.2

more general variant of the (28) for the inverse analysis, *i.e.*, to incorporate more complex nonlinear terms that are not present in the originals. In this paper, we focus on the misidentification between traveling wave solutions of the ZK equation and the RLW equation.

TABLE IV. The *misidentification* for the RLW equation.

	PDE	MSE ( $\times 10^{-6}$ )
Correct equation	$u_t + uu_x - (\nabla^2 u)_t + 0.0 (\nabla^2 u)_x = 0$	—
Identified $c = 2(1)$	$u_t + 0.9997uu_x - 2.0549 (\nabla^2 u)_t - 2.1105 (\nabla^2 u)_x = 0$	5.2
Identified $c = 2(2)$	$u_t + 0.9997uu_x - 1.0784 (\nabla^2 u)_t - 0.1579 (\nabla^2 u)_x = 0$	4.8
Identified $c = 1(3)$	$u_t + 0.9998uu_x - 0.8330 (\nabla^2 u)_t + 0.1666 (\nabla^2 u)_x = 0$	3.8
Identified $c = 1(4)$	$u_t + 0.9988uu_x - 0.9952 (\nabla^2 u)_t + 0.0030 (\nabla^2 u)_x = 0$	5.9

### C. Low PINNs resolution for the ZK and the RLW equations

We consider the following equation

$$u_t + \lambda_0 uu_x + \lambda_1 (\nabla^2 u)_t + \lambda_2 (\nabla^2 u)_x = 0. \quad (30)$$

We examine the inverse analysis for the data of the forward ZK and the RLW. Eq.(30) becomes the ZK equation for  $(\lambda_0, \lambda_1, \lambda_2) = (2.0, 0.0, 1.0)$  and, it reduces to the RLW equation for  $(\lambda_0, \lambda_1, \lambda_2) = (1.0, -1.0, 0.0)$ . As we already mentioned in Sec.2, the PINNs cannot distinguish these equations because they possess essentially the same traveling-wave solution  $u(t, x, y) = U(x - ct, y)$ . In Table III, we present the result of the identification of the ZK equation with the training data of the ZK vortex solution. Also, Table IV shows the identification of the RLW equation with the training data of the RLW vortex. It seems that both identifications are completely stuck.

In the following, we briefly look more closely at the origin of the stuck. Plugging the traveling-wave solution into Eq.(30), we obtain

$$-cU + \frac{\lambda_0}{2}U^2 + (\lambda_2 - c\lambda_1)\nabla^2 U = 0. \quad (31)$$

If Eq.(31) comes from the ZK Eq.(1), the coefficients should be

$$\lambda_0 = 2.0, \quad \lambda_2 - c\lambda_1 = 1.0, \quad (32)$$

while for the RLW Eq.(9) with  $u_x = 0$ , it is

$$\lambda_0 = 1.0, \quad \lambda_2 - c\lambda_1 = c. \quad (33)$$

Consequently,  $\lambda_1$  and  $\lambda_2$  cannot be uniquely determined. The reason for the problem is straightforward: Since the  $t$  derivatives and  $x$  derivatives for the traveling waves are convertible with one another, misinterpretation of the equation inevitably would arise in the PINNs analysis. If one wishes to efficiently use the PINNs, such coincidence must be suitably broken.

#### D. The conservative PINNs: The conservation constrained deep learning

Including the conserved quantities of the equations, ZK (5)-(8) or the RLW (14)-(17) into the *MSE* could potentially improve the resolution. Here we employ the second conserved quantity of the ZK

$$I_2(t) = \int \frac{u^2}{2} dx dy, \quad (34)$$

which is not the conserved quantity of the RLW equations because

$$\frac{dI_2(t)}{dt} = \int (u_x u_{xt} + u_y u_{yt}) dx dy \quad (35)$$

is not zero when we substitute the time derivative of (9) into the righthand side.

We define the cPINNs:the conserved PINNs algorithm which is realized by the following *MSE*

$$MSE := \mathcal{E} + C(\mathcal{E}) \sum_{N_c} |I_2^{\text{pred}} - I_2^{\text{correct}}|^2 \quad (36)$$

where the  $\mathcal{E}$  is identical to the standard *MSE* that was previously introduced for the forward problem (23)

$$\mathcal{E} = \frac{1}{N_u} \sum_{i=1}^{N_u} |u_{\text{pred}}^0(x^i, y^i, 0) - u_{\text{correct}}^0(x^i, y^i, 0)|^2 + \frac{1}{N_F} \sum_{i=1}^{N_F} |\mathcal{F}(x^i, y^i, t^i)|^2 + \frac{1}{N_b} \sum_{N_b} |BC|^2, \quad (37)$$

and for the inverse problem (27)

$$\mathcal{E} = \frac{1}{N_u} \sum_{i=1}^{N_u} |u_{\text{pred}}(x^i, y^i, t^i) - u_{\text{correct}}(x^i, y^i, 0)|^2 + \frac{1}{N_F} \sum_{i=1}^{N_F} |\tilde{\mathcal{F}}(x^i, y^i, t^i)|^2. \quad (38)$$

The  $N_c$  is the number of the reference time for evaluating the conserved quantity  $I_2$ ; Here we evaluate the integration at  $t = 0.0, 1.0, 2.0, 3.0, 4.0$  (i.e.,  $N_c = 5$ ) using the standard Simpson's method. To make the cPINNs even more efficient, the  $\mathcal{E}$  should be trained before the conservation law is taken into account. The weight function  $C(\mathcal{E})$  is defined in terms of a parameter  $\gamma$  and a critical value of  $\mathcal{E}_{\text{crit}}$  such that

$$C(\mathcal{E}) = \begin{cases} \exp(-\gamma \mathcal{E}_{\text{crit}}) & \mathcal{E} > \mathcal{E}_{\text{crit}} \\ \exp(-\gamma \mathcal{E}) & \mathcal{E} \leq \mathcal{E}_{\text{crit}}. \end{cases} \quad (39)$$

We show a typical behavior of the  $C(\mathcal{E})$  in Fig.4. It is clear that the regular PINNs predominate at first, and that the analysis shifts to the cPINNs at a later point since smaller  $\mathcal{E}$  increases the coefficient  $C(\mathcal{E})$ .

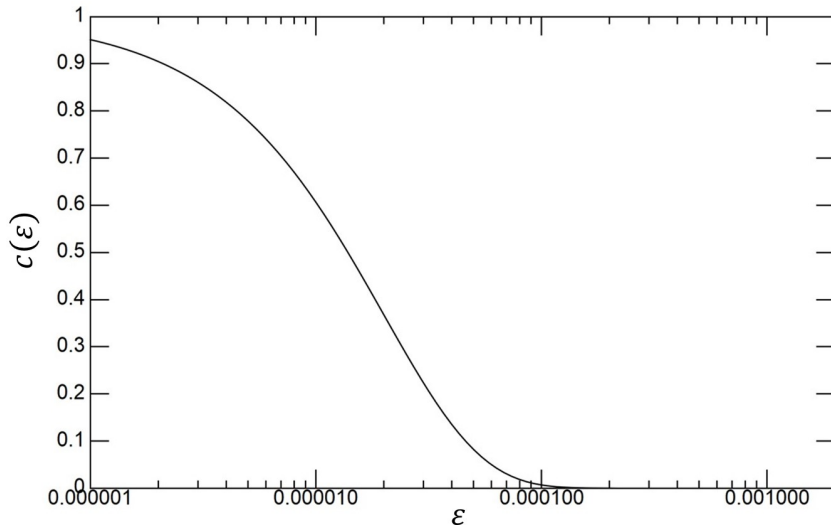


FIG. 4. The behavior of  $C(\mathcal{E})$  for  $\gamma = 5.0 \times 10^4$  and  $\mathcal{E}_{\text{crit}} = 1.0 \times 10^{-3}$ .

The profile of the single soliton via cPINNs is presented in Fig.5. To verify the accuracy of the cPINNs, we assess the variation from the numerical analysis:  $u_{\text{pred}} - u_{\text{correct}}$ , and the predictability of the cPINNs is much better than that of the PINNs analysis as we can see in Fig.6.

However, the cPINNs are ineffective at increasing the predictability of the inverse analysis. As shown in Table V, the cPINNs do not work, or perform even worse than the PINNs for identifying the equation of the predicted data. The main reason for the failure is that the cPINNs' projected profile is more accurate than that of PINNs and the output of the cPINNs is closer to  $u_{\text{pred}}(t, x, y) \sim U(x - ct, y)$ . Unfortunately, the misidentification may be the result of the improvement.

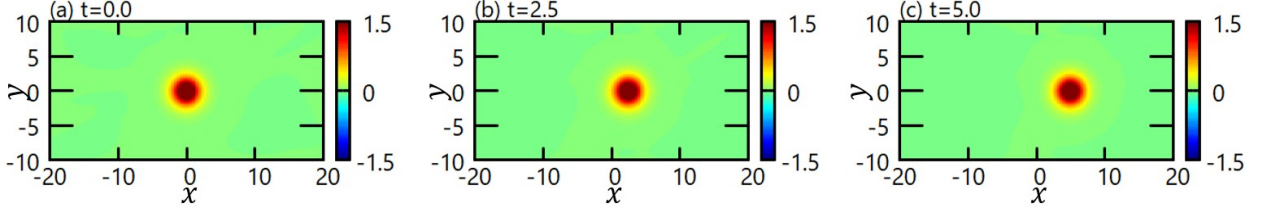


FIG. 5. single soliton profile predicted by cPINNs. the parameters for the  $C(\mathcal{E})$  are fixed as  $\gamma = 5.0 \times 10^4$ ,  $\mathcal{E}_{\text{crit}} = 1.0 \times 10^{-3}$ .

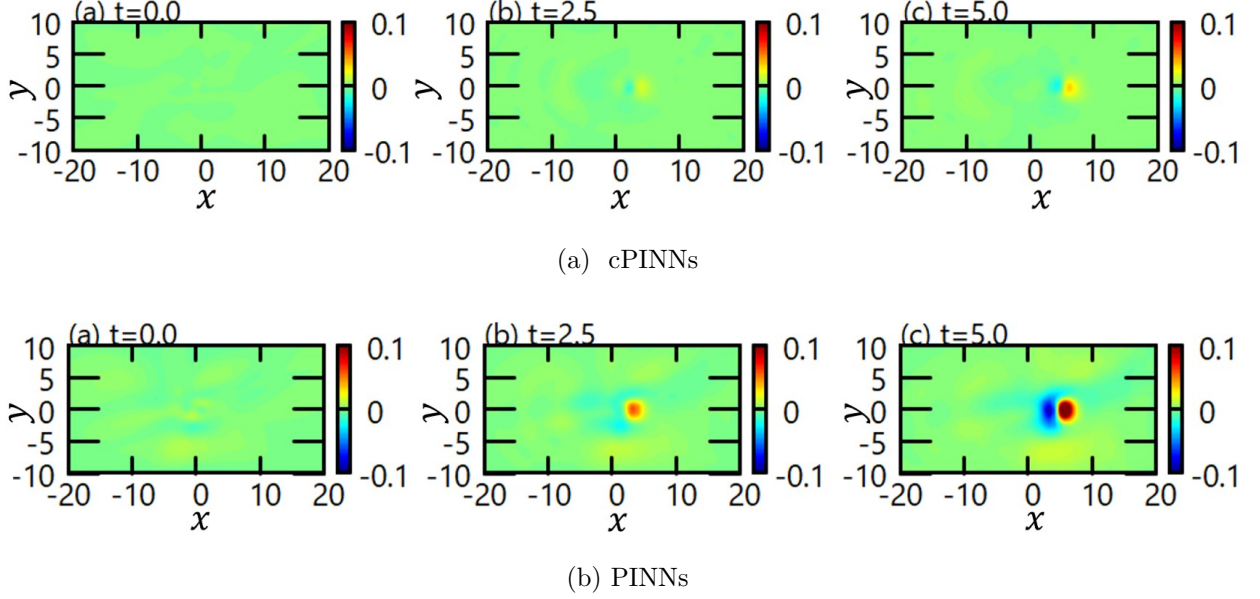


FIG. 6. The error between the predicted profile and the numerical solution:  $u_{\text{pred}} - u_{\text{correct}}$  of the (a) cPINNs, and (b) PINNs.

TABLE V. The identification of the ZK equation in the  $MSE$  (36) with changing the coupling parameter  $\alpha$ .

	$\gamma (\times 10^3)$	$PDE$	$MSE (\times 10^{-6})$
Correct equation	—	$u_t + 2uu_x + (\nabla^2 u)_x = 0$	—
Identified	50	$u_t + 2.019uu_x + 0.5659 (\nabla^2 u)_x - 0.4524 (\nabla^2 u)_t = 0$	2.0
Identified	10	$u_t + 2.020uu_x + 0.5648 (\nabla^2 u)_x - 0.4524 (\nabla^2 u)_t = 0$	2.0
Identified	5	$u_t + 2.020uu_x + 0.5676 (\nabla^2 u)_x - 0.4511 (\nabla^2 u)_t = 0$	2.2
Identified	1	$u_t + 0.6362uu_x + 0.0351 (\nabla^2 u)_x - 0.00913 (\nabla^2 u)_t = 0$	611

### E. The 2-soliton solution

For the next application, we consider the 2-soliton initial profile, because it induces a solution that inherently differs from a simple traveling wave solution. We only place the second profile far behind the first one which never collide with each other. We define the initial profile

$$u(0, x, y) = U_{c_1}(x - x_0, y) + U_{c_2}(x + x_0, y) \quad (40)$$

where  $c_1, c_2$  are the speed of each pulse, respectively. The initial profile breaks the coincidence of the  $x$  derivatives and the  $t$  derivatives. For the training data of the inverse analysis, we employ the segment data:  $t \in$  (a)  $[0.0, 3.3)$ , (b)  $[3.3, 6.6)$ , (c)  $[6.6, 9.9)$ , (d)  $[9.9, 13.3)$ , (e)  $[13.3, 16.6)$ , (f)  $[16.6, 19.9)$ , as plotted in Fig.7. The result of the inverse analysis is presented in Table VI. The resolutions seem certain to improve, but the  $MSEs$  still need to be fully converged. There's yet another major disadvantage in this scheme. It is now becoming evident that the PINNs inverse analysis loses the resolutions during the collision processes of solitons, and this might happen in this instance [64]. In the following section, we will discuss the novel prescriptions for improving resolution that do not rely on the dynamics of the 2-soliton.

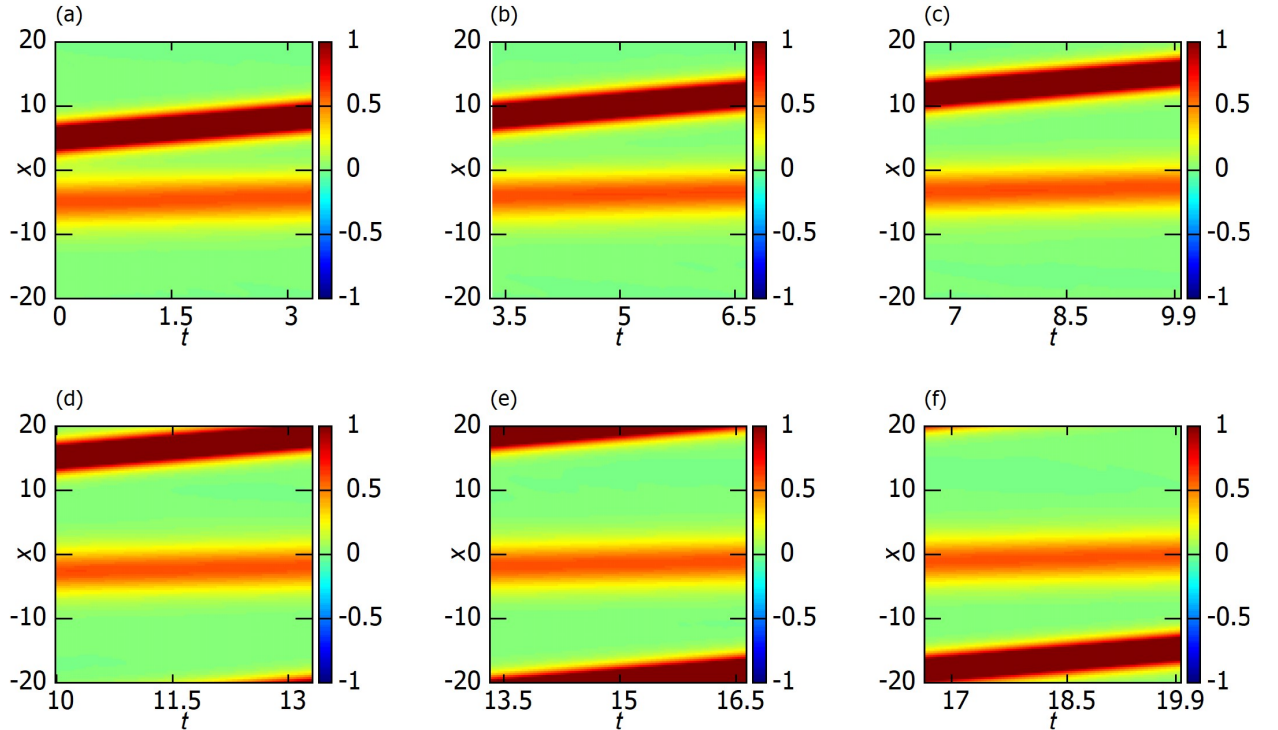


FIG. 7. 2-soliton training data of  $c_1 = 1.0, c_2 = 0.25, x_0 = 6.0$ . with the time segment of (a)  $t \in [0.0, 3.3)$ , (b)  $t \in [3.3, 6.6)$ , (c)  $t \in [6.6, 9.9)$ , (d)  $t \in [9.9, 13.3)$ , (e)  $t \in [13.3, 16.6)$ , (f)  $t \in [16.6, 19.9)$

TABLE VI. The identification of the ZK equation in terms of the 2-soliton with the small time segment data:  $t \in$  (a) [0.0, 3.3), (b) [3.3, 6.6), (c) [6.6, 9.9), (d) [9.9, 13.3), (e) [13.3, 16.6), (f) [16.6, 19.9).

	$PDE$	$MSE (\times 10^{-6})$
Correct equation	$u_t + 2uu_x + 0.0 (\nabla^2 u)_t + (\nabla^2 u)_x = 0$	—
Identified (a)	$u_t + 2.056uu_x - 0.001 (\nabla^2 u)_t + 1.058 (\nabla^2 u)_x = 0$	5.0
Identified (b)	$u_t + 2.046uu_x - 0.029 (\nabla^2 u)_t + 1.020 (\nabla^2 u)_x = 0$	5.3
Identified (c)	$u_t + 2.004uu_x - 0.026 (\nabla^2 u)_t + 1.014 (\nabla^2 u)_x = 0$	6.5
Identified (d)	$u_t + 2.032uu_x - 0.039 (\nabla^2 u)_t + 0.997 (\nabla^2 u)_x = 0$	8.3
Identified (e)	$u_t + 1.991uu_x - 0.021 (\nabla^2 u)_t + 0.996 (\nabla^2 u)_x = 0$	9.8
Identified (f)	$u_t + 2.050uu_x - 0.005 (\nabla^2 u)_t + 1.060 (\nabla^2 u)_x = 0$	5.5

#### IV. DATA-DRIVEN DISCOVERY OF THE GOVERNING EQUATIONS

In this section, we would like to examine the equations from the data of the single vortex with some non-trivial twists. It is unquestionably useful because observational data is invariably tainted by a variety of noises, modulations, and other disturbances while attempting to derive the governing equation using PINNs. We give a few examples that successfully identify the governing equations.

##### A. Deformation of the initial profile

One of the reasons for the misidentification is that we employed the traveling-wave solution of the normalized equation (13) as the initial profile. A nonlinear partial differential equation often has numerous independent solutions caused by differences in the initial conditions [44], providing deeper insight into the mathematical meanings of the equation and the phenomena of our concern. If we use the data with the different initial profiles in the PINNs analysis, the resolution improves because this prescription would break the condition  $\frac{\partial u}{\partial x} = -c \frac{\partial u}{\partial t}$ . The Gaussian profile

$$u(0, x, y) := 2.0 \exp \left[ -\frac{1}{\ell} (x^2 + y^2) \right], \quad (41)$$

is widely used in the analysis of several evolution equations in two-space dimensions. It can be an initial profile of the ZK and the RLW equations and we numerically solve these governing equations and get the data for the inverse analysis. We present the results for forward analysis of the ZK equation with the initial profiles (41) of the several scales  $\ell = 2.5, 5.0, 7.5$  and  $10.0$  in Figure 8. The results of the inverse analysis for the several data with  $\ell$  from 2.25 to 10.0 is given in Table VII.

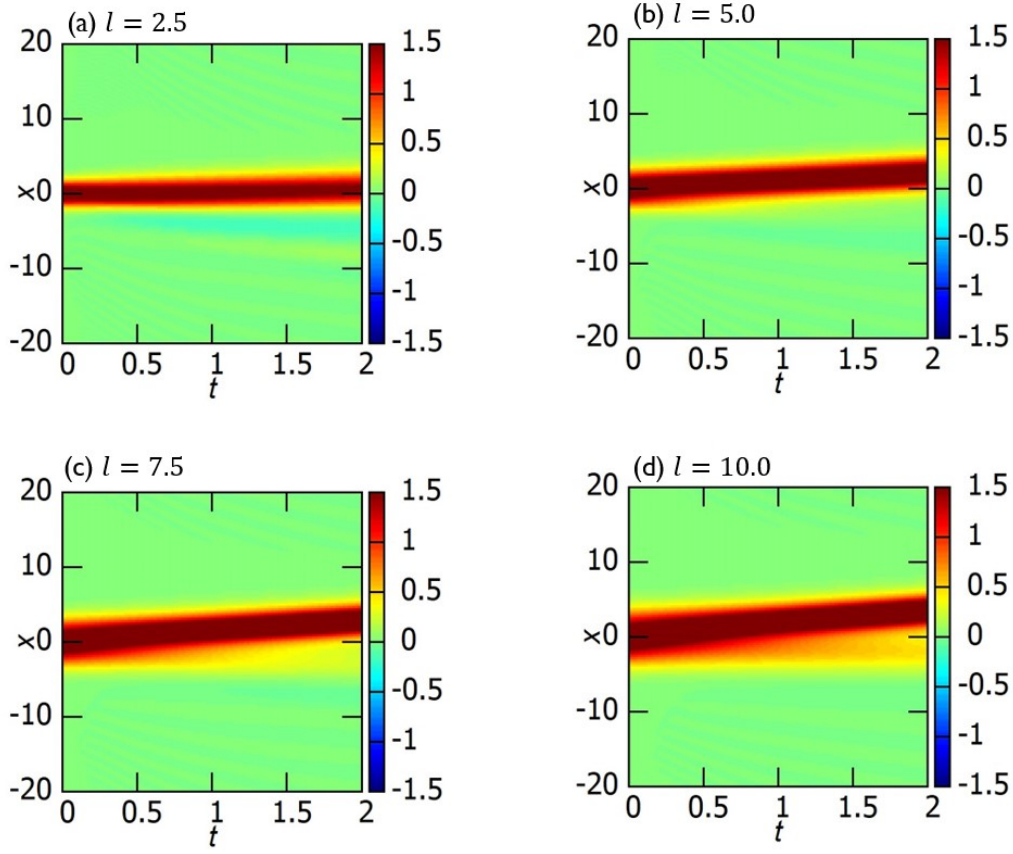


FIG. 8. The time evolution of the Gaussian profiles with  $\ell = 2.5, 5.0, 7.5$ , and  $10.0$

The results show that since the *MSE* further convergence has to be attained because the *MSE* is not small enough ( $\sim 10^{-5}$ ).

TABLE VII. The identification of the ZK equation using the data of the Gaussian initial profiles.

	<i>PDE</i>	<i>MSE</i> ( $\times 10^{-5}$ )
Correct equation	$u_t + 2uu_x + 0.0 (\nabla^2 u)_t + (\nabla^2 u)_x = 0$	—
Identified $\ell = 2.25$	$u_t + 1.986uu_x - 0.0581 (\nabla^2 u)_t + 0.9797 (\nabla^2 u)_x = 0$	6.1
Identified $\ell = 2.50$	$u_t + 2.0407uu_x - 0.0569 (\nabla^2 u)_t + 1.0106 (\nabla^2 u)_x = 0$	3.7
Identified $\ell = 2.75$	$u_t + 2.0558uu_x - 0.0771 (\nabla^2 u)_t + 1.0102 (\nabla^2 u)_x = 0$	2.3
Identified $\ell = 4.75$	$u_t + 2.0624uu_x - 0.1149 (\nabla^2 u)_t + 0.94666 (\nabla^2 u)_x = 0$	3.8
Identified $\ell = 5.0$	$u_t + 2.0599uu_x - 0.14533 (\nabla^2 u)_t + 0.92023 (\nabla^2 u)_x = 0$	3.0
Identified $\ell = 5.25$	$u_t + 2.05069uu_x - 0.06841 (\nabla^2 u)_t + 0.97961 (\nabla^2 u)_x = 0$	2.4
Identified $\ell = 7.25$	$u_t + 2.0534uu_x - 0.0475 (\nabla^2 u)_t + 0.9973 (\nabla^2 u)_x = 0$	1.8
Identified $\ell = 7.50$	$u_t + 2.05035uu_x - 0.04637 (\nabla^2 u)_t + 0.9950 (\nabla^2 u)_x = 0$	1.7
Identified $\ell = 7.75$	$u_t + 2.04880uu_x - 0.052728 (\nabla^2 u)_t + 0.9840 (\nabla^2 u)_x = 0$	2.0
Identified $\ell = 10.0$	$u_t + 2.0473uu_x - 0.0369 (\nabla^2 u)_t + 0.9976 (\nabla^2 u)_x = 0$	1.3

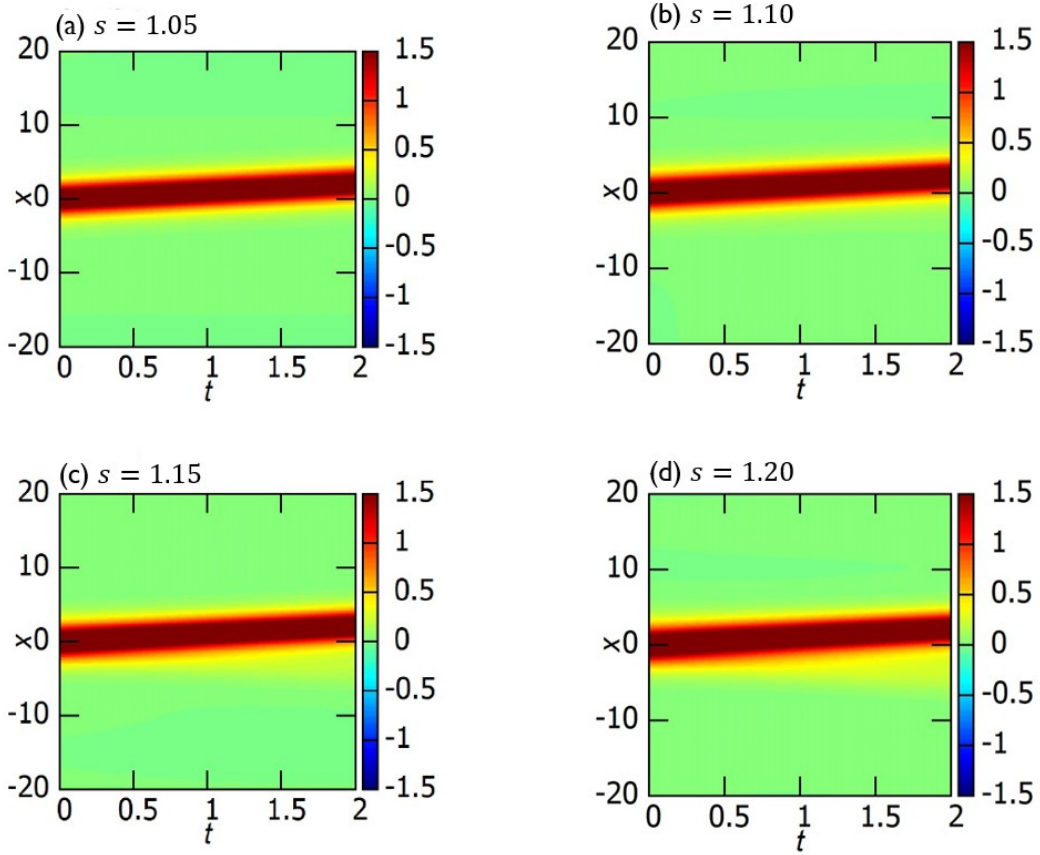


FIG. 9. The time evolution of the oval-shaped profiles with  $s = 1.05, 1.10, 1.15,$  and  $1.20$

Another option for choice of the initial condition might be more physical basis. In geophysical fluid dynamics like Jupiter's GRS, the oval-shaped profile is frequently seen and the ZK equation is a toy model of the intermediate geostrophic regime, which is believed to govern the GRS. We employ the following form of the initial condition

$$u(0, x, y) := U\left(s\xi, \frac{1}{s}y\right), \quad s > 1. \quad (42)$$

Again it breaks the coincidence  $\frac{\partial u}{\partial x} = -c\frac{\partial u}{\partial t}$ , then improves the PINNs' resolution. We present the results for forward analysis of the ZK equation with the initial profiles (42) of the several deformation parameters  $s = 1.05, 1.1, 1.15$  and  $1.20$  in Fig. 9. The results of the inverse analysis for the several data with  $s$  from  $1.0$  to  $1.2$  in Table VIII. Apparently, the predictive power of the PINNs is certainly improved for  $\beta > 1.125$ . We must admit that the current prescription has a downside in that excessive deformation often contaminates the vortex later on. The origin of the instability is that it inevitably violates the conservation laws. We conclude that while using deformed initial profiles is rather promising, it is only applicable in cases where there is little deviation from the circular shape.

TABLE VIII. The identification of the ZK equation with the data of the oval-shaped initial profiles.

	<i>PDE</i>	<i>MSE</i> ( $\times 10^{-6}$ )
Correct equation	$u_t + 2uu_x + 0.0 (\nabla^2 u)_t + (\nabla^2 u)_x = 0$	–
Identified $s = 1.000$	$u_t + 1.995uu_x - 0.0581 (\nabla^2 u)_t + 0.45367 (\nabla^2 u)_x = 0$	1.5
Identified $s = 1.025$	$u_t + 2.0140uu_x - 0.5489 (\nabla^2 u)_t + 0.45300 (\nabla^2 u)_x = 0$	3.4
Identified $s = 1.050$	$u_t + 2.0241uu_x - 0.4677 (\nabla^2 u)_t + 0.53675 (\nabla^2 u)_x = 0$	6.8
Identified $s = 1.075$	$u_t + 2.02010uu_x - 0.4754 (\nabla^2 u)_t + 0.51766 (\nabla^2 u)_x = 0$	11.8
Identified $s = 1.100$	$u_t + 2.0248uu_x - 0.3649 (\nabla^2 u)_t + 0.64731 (\nabla^2 u)_x = 0$	13.6
Identified $s = 1.125$	$u_t + 1.99602uu_x - 0.07228 (\nabla^2 u)_t + 0.92303 (\nabla^2 u)_x = 0$	9.5
Identified $s = 1.150$	$u_t + 2.00005uu_x - 0.08176 (\nabla^2 u)_t + 0.91783 (\nabla^2 u)_x = 0$	10.2
Identified $s = 1.175$	$u_t + 1.9961uu_x - 0.06765 (\nabla^2 u)_t + 0.92731 (\nabla^2 u)_x = 0$	13.0
Identified $s = 1.200$	$u_t + 1.9975uu_x - 0.03614 (\nabla^2 u)_t + 0.9611 (\nabla^2 u)_x = 0$	12.8

### B. A perturbative small friction via a background flow

Both the RLW and the ZK equations are governing equations of the plasma or the fluid dynamics. In fact, the former is a simplified form of the drift wave equation in plasma or the quasi-geostrophic Rossby waves in rotating fluid when we omit the Jacobian nonlinear term from the governing equation. The latter has a close connection with the intermediate geostrophic regime of the shallow water dynamics [26]. The equation possesses the anti-cyclonic stable vortex which is supposed to be a candidate of the GRS. For both the drift wave equation and the intermediate geostrophic equation, the existence of the sheared flows are crucial for finding the stable, long-lived solutions [26, 28, 65].

Our goal is to enhance the PINNs' performance by utilizing the influence of the background flow. For the purpose, we are based on the above intermediate geostrophic equation for finding the perturbative friction term. The equation for the cyclonic shear [26, 27] is

$$\frac{\partial \eta}{\partial t} + 2\eta \frac{\partial \eta}{\partial x} - \frac{\partial}{\partial x} (\nabla^2 \eta) + 2y \frac{\partial \eta}{\partial x} - 2J[\nabla^2 \eta, \eta] = 0 \quad (43)$$

The last term, the Jacobian is defined as  $J[A, B] := \partial_x A \partial_y B - \partial_y A \partial_x B$  which represents the geostrophic advection of vorticity in the words of fluid dynamics, and we refer to it as the vector nonlinear term. The stream function  $\eta := \eta(x, y, t)$  is expanded the sheared zonal flow current  $u_0(y)$  such as

$$\eta(x, y, t) = \int_0^y u_0(y') dy' + u(x, y, t). \quad (44)$$

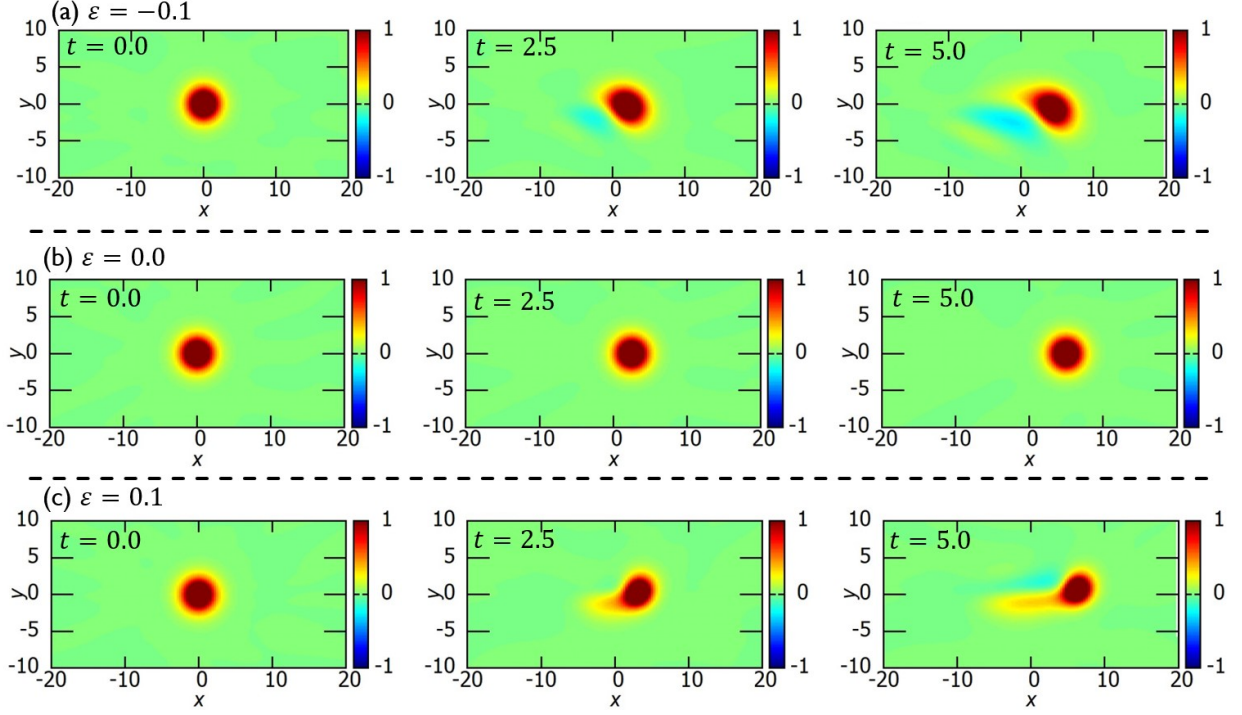


FIG. 10. The training data with constant flow  $u_0 = -1.0 + \varepsilon$ , where (a):  $\varepsilon = -0.1$ , (b):  $\varepsilon = 0.0$ , (c):  $\varepsilon = 0.1$ . where the field  $y$  is a perturbation from sole existence of the zonal flow. If we set  $u_0 = -1.0$  and omit the Jacobian and then, the equation becomes the ZK equation [28]. Introducing the constant current

$$u_0^1 := -1.0 + \varepsilon, \quad |\varepsilon| \ll 1, \quad (45)$$

we can write down (43) in terms of  $u$  such as

$$u_t + 2uu_x + (\nabla^2 u)_x - 2J[\nabla^2 u, u] + 2\varepsilon\{yu_x - (\nabla^2 u)_x\} = 0. \quad (46)$$

After the removal of the Jacobian (this is possible when a solution is close to circular shape), we identify the perturbative term of the following form

$$\varepsilon \mathcal{N}^1(u_x, u_{xxx}, u_{xyy}) := 2\varepsilon\{yu_x - (\nabla^2 u)_x\}. \quad (47)$$

Similarly, if we consider a  $y$ -dependent sheared current

$$u_0^2(y) := -1.0 + \varepsilon y, \quad |\varepsilon| \ll 1, \quad (48)$$

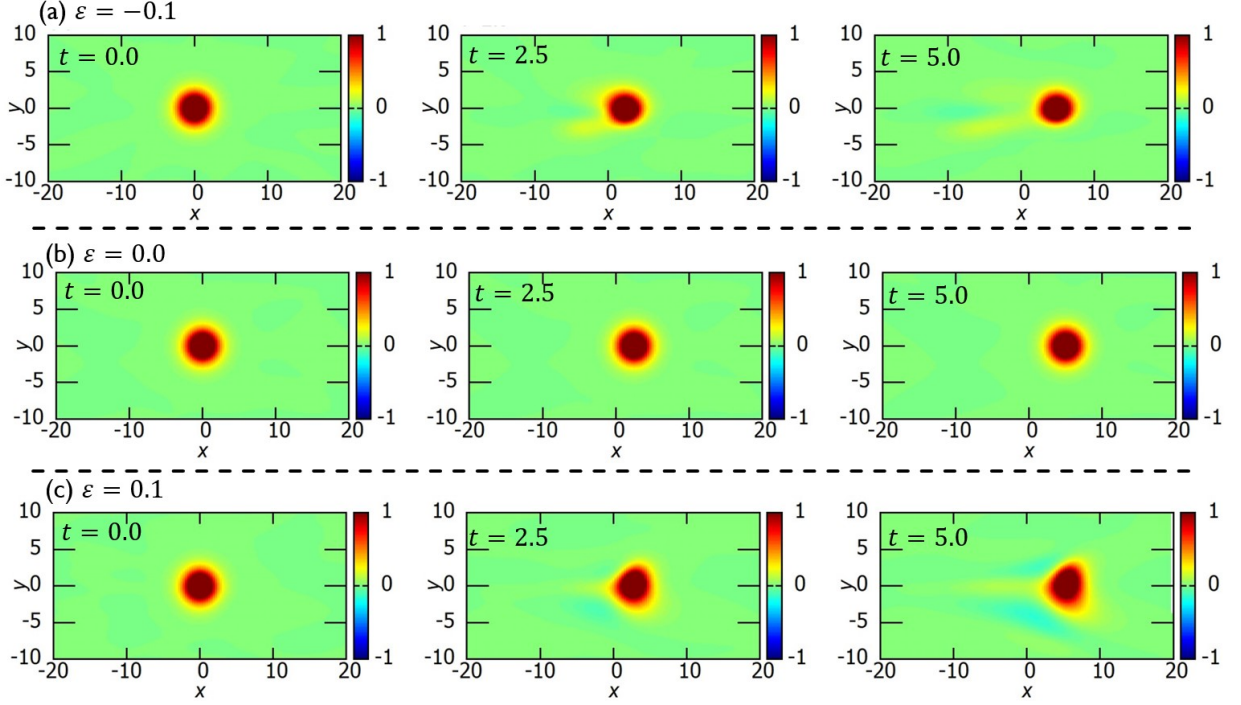


FIG. 11. The training data with  $y$ -dependent flow  $u_0 = -1.0 + \varepsilon y$ , where (a):  $\varepsilon = -0.1$ , (b):  $\varepsilon = 0.0$ , (c):  $\varepsilon = 0.1$ .

we find

$$\varepsilon \mathcal{N}^2(u_x, u_{xxx}, u_{xyy}) := \varepsilon \{y^2 u_x - 2y (\nabla^2 u)_x\}. \quad (49)$$

The modified ZK equation is defined as

$$\mathcal{F}_{\text{mZK}}^a = u_t + \mathcal{N}_{\text{ZK}}(u, u_x, u_{xxx}, u_{xyy}) + \varepsilon \mathcal{N}^a(u_x, u_{xxx}, u_{xyy}) = 0, \quad a = 1, 2 \quad (50)$$

Note that the equation of  $\mathcal{F}_{\text{mZK}}^1$  possesses four conserved quantities, where the first two  $I_1, I_2$  is completely same as the ZK equation while the  $I_3, I_4$  is slightly modified from (7), (8) such as

$$I_3' := \int \left[ (\nabla u)^2 - \frac{1}{1-2\varepsilon} \frac{1}{3} u^3 - \frac{\varepsilon}{1-2\varepsilon} y u^2 \right] dx dy, \quad (51)$$

$$I_4' := \int r u dx dy - t e_x \int (u^2 + 2\varepsilon y u) dx dy, \quad (52)$$

The  $I_3'$  corresponds to the total energy in  $\mathcal{F}_{\text{mZK}}^1$ . It is simply obtained by multiplying the Laplacian  $\nabla^2 u$  on the equation and using the doubly periodic boundary conditions to integrate through the whole area. It comprises the kinetic energy:  $(\nabla u)^2$ , a potential energy:  $u^3$ , and also a twisting

term:  $yu^2$ . Note that the  $|\varepsilon|$  is a small one so the denominators in (51) never become zero. The solutions of the equation  $\mathcal{F}_{\text{mZK}}^1$  are stable for the time evolution because the energy is conserved. On the other hand, the energy of the  $\mathcal{F}_{\text{mZK}}^2$  is not conserved and the solutions tend to be unstable. We present the results of the forward analysis of  $\mathcal{F}_{\text{mZK}}^1$  in Fig.10 and  $\mathcal{F}_{\text{mZK}}^2$  in Fig.11. Here we plot the solutions with the strength of the perturbative term  $\varepsilon = -1.0, 0.0$  and  $1.0$ .

The inverse analysis with the equation

$$\tilde{\mathcal{F}} = u_t + \bar{\mathcal{N}}(u, u_x, u_{txx}, u_{tyy}, u_{xxx}, u_{xyy}, \boldsymbol{\lambda}) + \epsilon \mathcal{N}_1(u_x, u_{xxx}, u_{xyy}) = 0 \quad (53)$$

$$\bar{\mathcal{N}}(u, u_x, u_{txx}, u_{tyy}, u_{xxx}, u_{xyy}, \lambda_0, \lambda_1, \lambda_2) := \lambda_0 uu_x + \lambda_1 (\nabla^2 u)_t + \lambda_2 (\nabla^2 u)_x \quad (54)$$

The results are shown in Fig.12. Using the results of the forward analysis for the solution of (50), we compute the mean square error of the model parameters defined as

$$\text{RMSE} := \sqrt{\frac{\sum_{i=0}^2 |\lambda_i^{\text{pred}} - \lambda_i^{\text{correct}}|^2}{3}} \quad (55)$$

we find that significant improvement in the accuracy is realized through the certain strength of the perturbation term of the constant current. However, the  $y$ -dependent current, which changes the original ZK equation into a non-conservative equation, cannot improve the predictability of the PINNs. As a result, we draw the conclusion that PINN predictability can be increased with a small perturbation that maintains the conservation laws.

## V. SUMMARY

In this paper, we have investigated the PINNs for the analysis of the quasi-integrable nonlinear differential equations: Zakharov-Kuznetsov equation and the regularized long-wave equation. These equations share some common structures for their traveling-wave solutions and then, the PINNs fail to identify them from the data. The identifications are improved by using the various beginning profiles, such as the Gaussian and the two-solitons, though the MSEs still need to be fully converged. The cPINNs, where the conservation laws are applied to the MSE, do not work in this analysis, because the strength of the conservation laws appears to be too low to enhance convergence. If the method eventually proves effective, we will require a more thorough investigation with substantial computational resources.

On the other hand, if we introduce a small perturbation, the friction term into the equation, the numerical convergence appears to be well and the identification turns out to be significantly

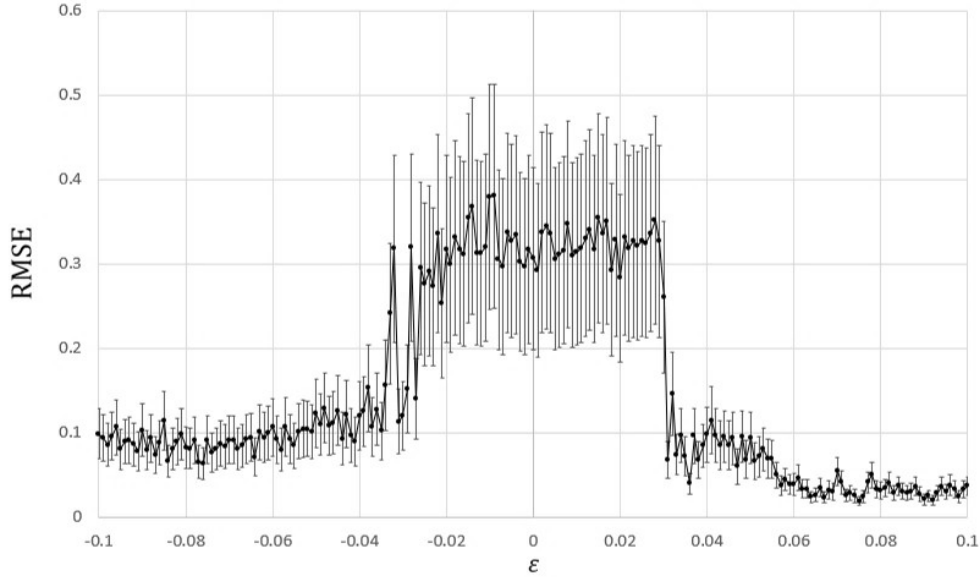
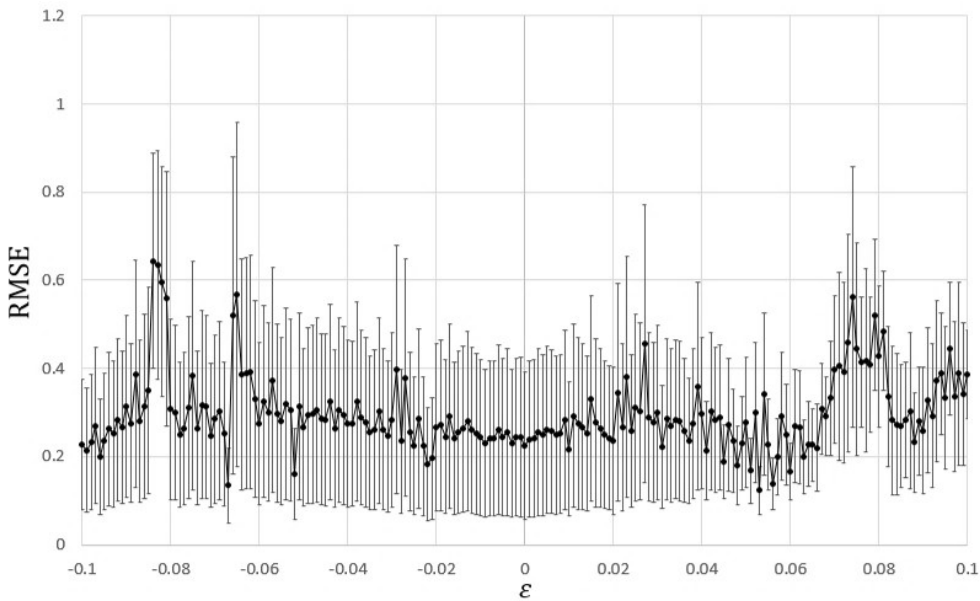
(a)  $u_0 := -1.0 + \varepsilon$ (b)  $u_0 := -1.0 + \varepsilon y$ 

FIG. 12. Relation between the accuracy of the identification and strength of the perturbative term induced to the ZK equation  $\varepsilon$ . The root mean square error:  $\text{RMSE} \sqrt{\frac{\sum_{i=0}^2 |\lambda_i^{\text{pred}} - \lambda_i^{\text{correct}}|^2}{3}}$  is: (a) suppressed for  $\varepsilon \gtrsim 0.05$  in case of the constant current, (b) ineffective suppression of the RMSE in the case of the  $y$ -dependent current.

better than the other approaches. Especially, it works very well when the friction term keeps a number of the conservation laws.

Our ultimate objective is to use the PINNs technology to discover the most appropriate governing equation of the GRS in terms of various observational data or phenomenological considerations. If we encounter a problem similar to the one described above, it should be resolved using some of the minor perturbations covered in this study.

**Acknowledgments** The authors would like to thank Satoshi Horihata, Kiori Obuse, Hiroshi Kakuhata, Ryu Sasaki, Filip Blaschke and Paweł Klimas for many useful advices and comments. N.S. and K.S. would like to thank all the conference organizers of QTS12 and Prof. Āestmir Burdík for the hospitality and also many kind considerations. K.S. was supported by Tokyo University of Science. A.N., N.S. and K.T. were supported in part by JSPS KAKENHI Grant Number JP23K02794.

## APPENDIX A: TECHNICAL SETUP OF THE PHYSICS-INFORMED NEURAL NETWORKS

Our analysis of the PINNs in this paper is based on a neural network consisting of 4 hidden layers, each containing 20 nodes. In order to fix the optimal parameters for both layers and nodes, here we solve the inverse problem of the ZK equation

$$u_t + \lambda_1 uu_x + \lambda_2 (\nabla^2 u)_x = 0. \tag{56}$$

for changing the number of layers or nodes. In Fig.13, we study the convergence property of the PINNs from 4 to 8 layers. It indicates that the result of the 6 layer is best choice for the convergence. Table IX is ability of the parameter prediction where the 4 layer looks better than the other number of the layers. The findings imply that selecting the layers is not as crucial as one may think to achieve better solutions.

Next, we study the appropriate size of the training data in the inverse analysis. We employ the range of the coordinates are set as  $x \in [-20, 20]$ ,  $y \in [-10, 10]$ ,  $t \in [0.0, 5.0]$  and the mesh number is set as  $N_x = 200$ ,  $N_y = 200$ ,  $N_t = 1000$ . The whole number of the training data becomes  $4 \times 10^7$  in this setup. Due to computational resource limits, we are unable to use the whole data set for the PINNs analysis; instead, we are forced to select the data's collocation points at random. Surprisingly, Table X indicates that the PINNs do not lose their predictability even if it learns only

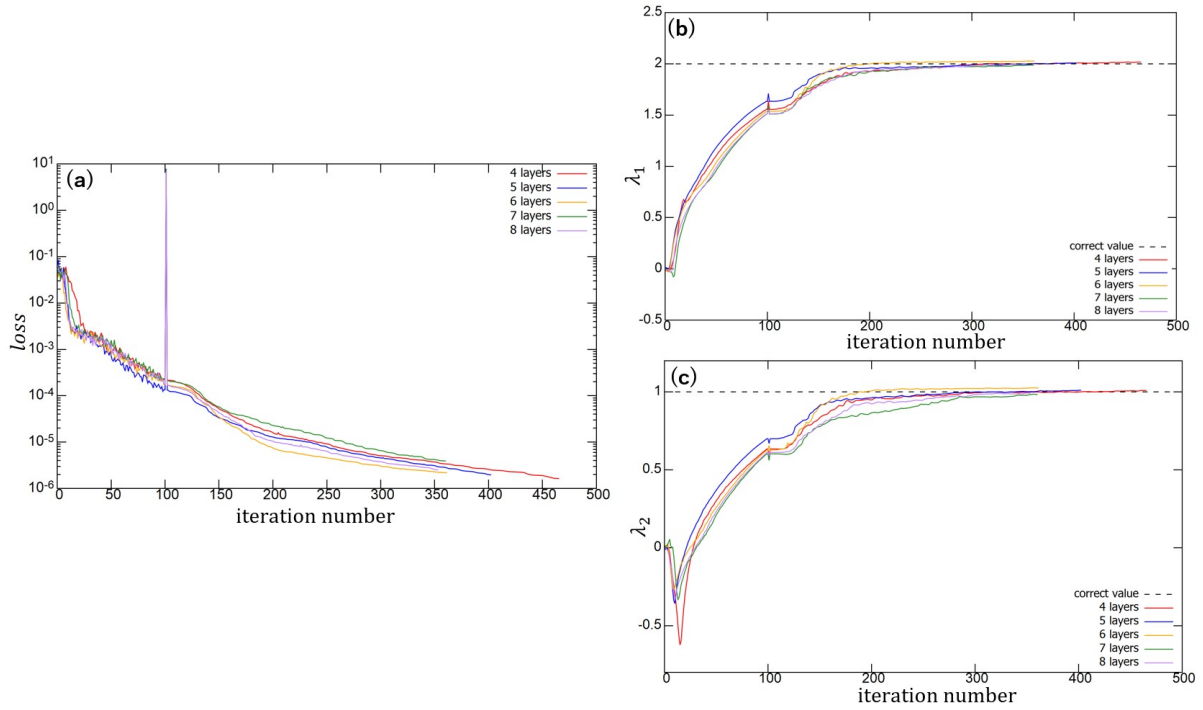


FIG. 13. The convergence of the loss function and the parameters of the ZK eq: (a) the MSE, (b) the predicted parameter of  $\lambda_1$ , (c) the predicted parameter of  $\lambda_2$

TABLE IX. The accuracy of the parameter prediction.

layers	$\lambda_1$	$\lambda_2$
4	2.01547	1.00873
5	2.00811	1.01046
6	2.02570	1.02479
7	1.98557	0.98272
8	2.00094	0.99105

0.0125% of its whole data. In this paper, we always use 25000 points(0.0625% of its whole data) as the training data.

TABLE X. The predictability for the parameters  $\lambda_1, \lambda_2$  of the inverse analysis for the choice of the training data points (and the ratio to the whole data).

training points (ratio)	$\lambda_1$	$\lambda_2$
5000 (0.0125%)	2.00185	0.99356
10000 (0.025%)	2.01124	1.01236
15000 (0.0375%)	2.01065	1.00369
20000 (0.05%)	1.99789	1.00730
25000 (0.0625%)	2.01291	1.01996
30000 (0.075%)	2.00883	1.00784
35000 (0.0875%)	2.01950	1.01835

## REFERENCES

- 
- [1] Maziar Raissi, Paris Perdikaris, and George Karniadakis, “Physics informed deep learning (part i): Data-driven solutions of nonlinear partial differential equations,” (2017), 10.48550/arXiv.1711.10561.
- [2] Maziar Raissi, Paris Perdikaris, and George Karniadakis, “Physics informed deep learning (part ii): Data-driven discovery of nonlinear partial differential equations,” (2017), 10.48550/arXiv.1711.10566.
- [3] M. Raissi, P. Perdikaris, and G.E. Karniadakis, “Physics-informed neural networks: A deep learning framework for solving forward and inverse problems involving nonlinear partial differential equations,” *Journal of Computational Physics* **378**, 686–707 (2019).
- [4] Maziar Raissi, Alireza Yazdani, and George Em Karniadakis, “Hidden fluid mechanics: Learning velocity and pressure fields from flow visualizations,” *Science* **367**, 1026–1030 (2020), <https://www.science.org/doi/pdf/10.1126/science.aaw4741>.
- [5] Steven L. Brunton, Bernd R. Noack, and Petros Koumoutsakos, “Machine learning for fluid mechanics,” *Annual Review of Fluid Mechanics* **52**, 477–508 (2020).
- [6] Teeratorn Kadeethum, Thomas M. Jorgensen, and Hamidreza M. Nick, “Physics-informed neural networks for solving nonlinear diffusivity and biot’s equations,” *PLOS ONE* **15**, 1–28 (2020).
- [7] Shengze Cai, Zhiping Mao, Zhicheng Wang, Minglang Yin, and George Em Karniadakis, “Physics-informed neural networks (pinns) for fluid mechanics: a review,” *Acta Mechanica Sinica* (2021), 10.1007/s10409-021-01148-1.
- [8] Kashinath K et al., “Physics-informed machine learning: case studies for weather and climate modeling,” *Phil.Trans.R.Soc.A* **379**, 20200093 (2021).
- [9] X. Jin, S. Cai, H. Li, and G.E. Karniadakis, “NSFnets (NavierStokes flow nets): Physics-informed

- neural networks for the incompressible Navier-Stokes equations,” *Journal of Computational Physics* **426**, 109951 (2021).
- [10] Rahul Rai and Chandan K. Sahu, “Driven by data or derived through physics? a review of hybrid physics guided machine learning techniques with cyber-physical system (cps) focus,” *IEEE Access* **8**, 71050–71073 (2020).
- [11] Hao Wu, Feliks Nüske, Fabian Paul, Stefan Klus, Péter Koltai, and Frank Noé, “Variational Koopman models: Slow collective variables and molecular kinetics from short off-equilibrium simulations,” *The Journal of Chemical Physics* **146**, 154104 (2017), [https://pubs.aip.org/aip/jcp/article-pdf/doi/10.1063/1.4979344/14899047/154104.1\\_online.pdf](https://pubs.aip.org/aip/jcp/article-pdf/doi/10.1063/1.4979344/14899047/154104.1_online.pdf).
- [12] Georgios Kissas, Yibo Yang, Eileen Hwuang, Walter R. Witschey, John A. Detre, and Paris Perdikaris, “Machine learning in cardiovascular flows modeling: Predicting arterial blood pressure from non-invasive 4d flow mri data using physics-informed neural networks,” *Computer Methods in Applied Mechanics and Engineering* **358**, 112623 (2020).
- [13] Carlos Ruiz Herrera, Thomas Grandits, Gernot Plank, Paris Perdikaris, and Simone Sahli Costabal, Francisco and Pezzuto, “Physics-informed neural networks to learn cardiac fiber orientation from multiple electroanatomical maps,” *Engineering with Computers* **38**, 3957–3973 (2022).
- [14] Kaan Sel, Amirmohammad Mohammadi, Roderic I. Pettigrew, and Roozbeh Jafari, “Physics-informed neural networks for modeling physiological time series for cuffless blood pressure estimation,” *npj Digital Medicine* **6**, 110 (2023).
- [15] Zhiwei Fang and Justin Zhan, “A physics-informed neural network framework for pdes on 3d surfaces: Time independent problems,” *IEEE Access* **8**, 26328–26335 (2020).
- [16] Francisco Sahli Costabal, Simone Pezzuto, and Paris Perdikaris, “Delta-pinns: Physics-informed neural networks on complex geometries,” *Engineering Applications of Artificial Intelligence* **127**, 107324 (2024).
- [17] Ameya D. Jagtap, Ehsan Kharazmi, and George Em Karniadakis, “Conservative physics-informed neural networks on discrete domains for conservation laws: Applications to forward and inverse problems,” *Computer Methods in Applied Mechanics and Engineering* **365**, 113028 (2020).
- [18] Siddhartha Mishra and Roberto Molinaro, “Physics informed neural networks for simulating radiative transfer,” *Journal of Quantitative Spectroscopy and Radiative Transfer* **270**, 107705 (2021).
- [19] Xingzhuo Chen, David J. Jeffery, Ming Zhong, Levi D. McClenny, Ulisses M. Braga-Neto, and Lifan Wang, “Using physics informed neural networks for supernova radiative transfer simulation,” (2022).
- [20] Yu Yang, Helin Gong, Shiquan Zhang, Qihong Yang, Zhang Chen, Qiaolin He, and Qing Li, “A data-enabled physics-informed neural network with comprehensive numerical study on solving neutron diffusion eigenvalue problems,” *Annals of Nuclear Energy* **183**, 109656 (2023).
- [21] Alexandr Sedykh, Maninadh Podapaka, Asel Saginalieva, Karan Pinto, Markus Pflitsch, and Alexey Melnikov, “Hybrid quantum physics-informed neural networks for simulating computational fluid dynamics in complex shapes,” *Machine Learning: Science and Technology* **5**, 025045 (2024).

- [22] Shuning Lin and Yong Chen, “A two-stage physics-informed neural network method based on conserved quantities and applications in localized wave solutions,” *Journal of Computational Physics* **457**, 111053 (2022).
- [23] Gang-Zhou Wu, Yin Fang, Nikolay A. Kudryashov, Yue-Yue Wang, and Chao-Qing Dai, “Prediction of optical solitons using an improved physics-informed neural network method with the conservation law constraint,” *Chaos, Solitons and Fractals* **159**, 112143 (2022).
- [24] Marzia Parisi, Yohai Kaspi, Galanti. Eli, Daniele Durante, Scott J. Bolton, Levin. Steven M., Dustin R. Buccino, Leigh N. Fletcher, Folkner. William M., Tristan Guillot, Ravit Helled, Iess. Luciano, Cheng Li, Kamal Oudrhiri, and Michael H. Wong, “The depth of jupiter’s great red spot constrained by juno gravity overflights,” *Science* **374**, 964–968 (2021).
- [25] Akira Hasegawa and Kunioki Mima, “Pseudo-three-dimensional turbulence in magnetized nonuniform plasma,” *The Physics of Fluids* **21**, 87–92 (1978).
- [26] Gareth Williams and Toshio Yamagata, “Geostrophic Regimes, Intermediate Solitary Vortices and Jovian Eddies,” *Journal of The Atmospheric Sciences - J ATMOS SCI* **41**, 453–478 (1984).
- [27] Jule G. Charney and Glenn R. Flierl, “Oceanic analogues of large-scale atmospheric motions,” *Evolution of physical oceanography* **504**, 548 (1981).
- [28] Yukito Koike, Atsushi Nakamura, Akihiro Nishie, Kiori Obuse, Nobuyuki Sawado, Yamato Suda, and Kouichi Toda, “Mock-integrability and stable solitary vortices,” *Chaos Solitons and Fractals: the interdisciplinary journal of Nonlinear Science and Nonequilibrium and Complex Phenomena* **165**, 112782 (2022), arXiv:2204.01985 [math-ph].
- [29] Jun Li and Yong Chen, “A deep learning method for solving third-order nonlinear evolution equations,” *Communications in Theoretical Physics* **72**, 115003 (2020).
- [30] Yin Fang, Gang-Zhou Wu, Nikolay A. Kudryashov, Yue-Yue Wang, and Chao-Qing Dai, “Data-driven soliton solutions and model parameters of nonlinear wave models via the conservation-law constrained neural network method,” *Chaos, Solitons and Fractals* **158**, 112118 (2022).
- [31] J.C.Pu and Y.Chen, “Lax pairs informed neural networks solving integrable systems,” *J. Comput. Phys.* **510**, 113090 (2024).
- [32] Zhou Huijuan, “Parallel Physics-Informed Neural Networks Method with Regularization Strategies for the Forward-Inverse Problems of the Variable Coefficient Modified KdV Equation,” *J. Syst. Sci. Complex.* **37**, 511–544 (2024).
- [33] Shuning Lin and Yong Chen, “Physics-informed neural network methods based on miura transformations and discovery of new localized wave solutions,” *Physica D: Nonlinear Phenomena* **445**, 133629 (2023).
- [34] Zijian Zhou and Zhenya Yan, “Solving forward and inverse problems of the logarithmic nonlinear schrödinger equation with pt-symmetric harmonic potential via deep learning,” *Physics Letters A* **387**, 127010 (2021).
- [35] Juncai Pu, Jun Li, and Yong and Chen, “Solving localized wave solutions of the derivative nonlinear

- schrödinger equation using an improved pinn method,” *Nonlinear Dynamics* **105**, 1723–1739 (2021).
- [36] Z.W.Miao and Y.Chen, “Physics-informed neural networks method in high-dimensional integrable systems,” *Mod.Phys.Lett.B.* **36(1)**, 2150531 (2022).
- [37] Zijian Zhou, Li Wang, and Zhenya Yan, “Deep neural networks learning forward and inverse problems of two-dimensional nonlinear wave equations with rational solitons,” *Computers and Mathematics with Applications* **151**, 164–171 (2023).
- [38] Li Wang, Zijian Zhou, and Zhenya Yan, “Data-driven vortex solitons and parameter discovery of 2d generalized nonlinear schrödinger equations with a pt-symmetric optical lattice,” *Computers and Mathematics with Applications* **140**, 17–23 (2023).
- [39] Genming Bai, Ujjwal Koley, Siddhartha Mishra, and Roberto Molinaro, “Physics informed neural networks (pinns) for approximating nonlinear dispersive pdes,” *Journal of Computational Mathematics* **39**, 816–847 (2021).
- [40] Z.Y. Yan Z.J. Zhou, L. Wang, “Deep neural networks learning forward and inverse problems of two-dimensional nonlinear wave equations with rational solitons,” *Comput. Math. Appl.* **151**, 164–171 (2023).
- [41] Li Wang and Zhenya Yan, “Data-driven rogue waves and parameter discovery in the defocusing nonlinear schrödinger equation with a potential using the pinn deep learning,” *Physics Letters A* **404**, 127408 (2021).
- [42] Jiaheng Li and Biao Li, “Mix-training physics-informed neural networks for the rogue waves of nonlinear schrödinger equation,” *Chaos, Solitons and Fractals* **164**, 112712 (2022).
- [43] Wei-Qi Peng, Jun-Cai Pu, and Yong Chen, “Pinn deep learning method for the chen-lee-liu equation: Rogue wave on the periodic background,” *Communications in Nonlinear Science and Numerical Simulation* **105**, 106067 (2022).
- [44] Yikai Chen, Hongli Xiao, Xiao Teng, Wenjun Liu, and Long Lan, “Enhancing accuracy of physically informed neural networks for nonlinear schrödinger equations through multi-view transfer learning,” *Information Fusion* **102**, 102041 (2024).
- [45] Junchao Chen, Jin Song, Zijian Zhou, and Zhenya Yan, “Data-driven localized waves and parameter discovery in the massive thirring model via extended physics-informed neural networks with interface zones,” *Chaos, Solitons and Fractals* **176**, 114090 (2023).
- [46] V. Zakharov and E A. Kuznetsov, “Three-dimensional solitons,” *Soviet Physics JETP* **29**, 594–597 (1974).
- [47] Hiroshi Iwasaki, Sadayoshi Toh, and Takuji Kawahara, “Cylindrical quasi-solitons of the Zakharov-Kuznetsov equation,” *Physica D: Nonlinear Phenomena* **43**, 293–303 (1990).
- [48] V. I. Petviashvili and V. V. Yan’kov, “Bilayer vortices in rotating stratified fluid,” *Dokl. Akad. Nauk SSSR* **267**, 825–828 (1982).
- [49] Christian Klein, Svetlana Roudenko, and Nikola Stoilov, “Numerical study of Zakhavor-Kuznetsov equations in two dimensions,” *Journal of Nonlinear Science* **31**, 1–28 (2021).

- [50] D. H. Peregrine, “Calculations of the development of an undular bore,” *Journal of Fluid Mechanics* **25**, 321–330 (1966).
- [51] Thomas Brooke Benjamin, J. L. Bona, and J. J. Mahony, “Model equations for long waves in nonlinear dispersive systems,” *Philosophical Transactions of the Royal Society of London. Series A, Mathematical and Physical Sciences* **272**, 47–78 (1972).
- [52] Takuji Kawahara, Keisuke Araki, and Sadayoshi Toh, “Interactions of two-dimensionally localized pulses of the regularized-long-wave equation,” *Physica D: Nonlinear Phenomena* **59**, 79–89 (1992).
- [53] Kh.O. Abdulloev, I.L. Bogolubsky, and V.G. Makhankov, “One more example of inelastic soliton interaction,” *Physics Letters A* **56**, 427–428 (1976).
- [54] J. Courtenay Lewis and J.A. Tjon, “Resonant production of solitons in the rlw equation,” *Physics Letters A* **73**, 275–279 (1979).
- [55] F. ter Braak, L. A. Ferreira, and W. J. Zakrzewski, “Quasi-integrability of deformations of the KdV equation,” *Nucl. Phys. B* **939**, 49–94 (2019), arXiv:1710.00918 [hep-th].
- [56] Atsushi Nakamura, Kiori Obuse, Nobuyuki Sawado, Kohei Shimasaki, and Kouichi Toda, “Machine learning study through physics-informed neural networks: Analysis of the stable vortices in quasi-integrable systems,” *Journal of Physics: Conference Series* **2667**, 012079 (2023), <https://dx.doi.org/10.1088/1742-6596/2667/1/012079>.
- [57] L. A. Ferreira, G. Luchini, and Wojtek J. Zakrzewski, “The concept of quasi-integrability,” *AIP Conf. Proc.* **1562**, 43–49 (2013), arXiv:1307.7722 [hep-th].
- [58] E.A. Kuznetsov, A.M. Rubenchik, and V.E. Zakharov, “Soliton stability in plasmas and hydrodynamics,” *Physics Reports* **142**, 103–165 (1986).
- [59] Katuhiko Goda and Yoshinari Fukui, “Numerical studies of the regularized long wave equation,” *Journal of the Physical Society of Japan* **48**, 623–630 (1980), <https://doi.org/10.1143/JPSJ.48.623>.
- [60] L. A. Medeiros and G. Perla Menzala, “Existence and uniqueness for periodic solutions of the benjamin-bona-mahony equation,” *SIAM Journal on Mathematical Analysis* **8**, 792–799 (1977), <https://doi.org/10.1137/0508062>.
- [61] D. Bhardwaj and R. Shankar, “A computational method for regularized long wave equation,” *Computers and Mathematics with Applications* **40**, 1397–1404 (2000).
- [62] Mehdi Dehghan and Rezvan Salehi, “The solitary wave solution of the two-dimensional regularized long-wave equation in fluids and plasmas,” *Computer Physics Communications* **182**, 2540–2549 (2011).
- [63] Mehdi Dehghan, Mostafa Abbaszadeh, and Akbar Mohebbi, “The use of interpolating element-free galerkin technique for solving 2d generalized benjamin-bona-mahony-burgers and regularized long-wave equations on non-rectangular domains with error estimate,” *Journal of Computational and Applied Mathematics* **286**, 211–231 (2015).
- [64] Atsushi Nakamura, Kiori Obuse, Nobuyuki Sawado, Kohei Shimasaki, Junichiro Shimazaki, and Kouichi Toda, to be published (2024).
- [65] G.G. Sutyryn and T. Radko, “Why the most long-lived oceanic vortices are found in the subtropical

westward flows,” *Ocean Modelling* **161**, 101782 (2021).